A new method deriving sea spray optical properties from multi-sensor spaceborne observations

K. W. Dawson[1], N. Meskhidze[1], D. Josset[2], and S. Gassó[3]

[1]Marine, Earth, and Atmospheric Science, North Carolina State University, Raleigh, NC, USA
[2]Science Systems and Applications, Inc/NASA Langley Research center
[3]GESTAR/Morgan State University, Goddard Space Flight Center, Greenbelt, Maryland

Correspondence to: Nicholas Meskhidze (nmeskhidze@ncsu.edu)

Abstract

Retrievals of aerosol optical depth (AOD) from the Cloud-Aerosol Lidar with Orthogonal Polarization (CALIOP) satellite sensor require the assumption of the extinction-to-backscatter ratio, also known as the lidar ratio. This paper evaluates a new method to calculate the lidar ratio of sea spray aerosol using two independent sources: the AOD from the Synergized Optical Depth of Aerosols (SODA) algorithm and the integrated attenuated backscatter from CALIOP. With this method, the particulate lidar ratio can be derived for individual CALIOP retrievals in single aerosol layer columns over the ocean. Global analyses are carried out using CALIOP level 2, 5km sea spray aerosol layer products and the collocated SODA nighttime data from December 2007 to February 2010. The global mean lidar ratio for sea spray aerosols was found to be 26 sr, roughly 30% higher than the current value prescribed by CALIOP standard retrieval algorithm. Data analysis also showed considerable spatiotemporal variability in the calculated lidar ratio over the remote oceans. The calculated aerosol lidar ratios are shown to be inversely related to the mean ocean surface wind speed: increase in ocean surface wind speed (U_{10}) from 0 to >15 ms^{-1} reduces the mean lidar ratios for sea spray particles from 32 sr (for $0 < U_{10} < 4$ ms^{-1}) to 22 sr (for $U_{10} > 15$ ms^{-1}). Such changes in the lidar ratio are expected to have a corresponding effect on the sea spray AOD. The outcomes of this study are relevant for future improvements of the SODA and CALIOP operational product and could lead to more accurate retrievals of sea spray AOD.

1 Introduction

Radiative forcing by sea spray aerosol (SSA) comprises a significant portion of the global energy budget. Studies have shown that the contribution of SSA to aerosol optical depth (AOD) is approximately 0.15 and likewise, the contribution of SSA to cloud condensation nuclei (CCN) is about 60 cm^{-3} (Kaufman et al., 2002; Lewis and Schwartz, 2004) . Thus, SSA is an important natural aerosol affecting both direct (i.e., extinction of solar radiation via scattering and absorption) and indirect (i.e., cloud lifetime and frequency) radiative forcing of climate. As SSA contributes substantially to the preindustrial, natural background and provides the base line on top of which anthropogenic forcing should be quantified, it is very important to properly characterise SSA burden and its spatiotemporal distribution. The representation of SSA in climate models was shown to strongly influence the predicted impact of anthropogenic aerosols on climate via direct and indirect effects (Ghan et al., 2001; Hoose et al., 2009; Wang and Penner, 2009; Meskhidze et al., 2011; Westervelt et al., 2012). Furthermore, uncertainties in preindustrial aerosol, of which sea spray is a part of, were shown to contribute up to 45% in the overall variance in radiative forcing (Carslaw et al., 2013).

Aerosols over the remote oceans consist mainly of a mixture of marine (e.g., primary sea spray particles and sulfates from the oxidation of dimethylsulfide), natural continental (e.g., mineral dust and biomass burning), and human-induced pollution (Andreae, 2007). Therefore, knowing horizontal and vertical distribution, as well as speciation of aerosols becomes extremely important for the correct quantification of SSA radiative properties. The last decade has produced a large body of information regarding the sources and composition of marine aerosols, resulting in a reassessment of the complex role that sea spray particles play in climate and various geophysical phenomena. Passive satellite instruments like the Sea-Viewing Wide Field-of-view Sensor (SeaWiFS), the MODerate resolution Imaging Spectroradiometer (MODIS), and the Multi-angle Imaging Spectroradiometer (MISR), as well as the ground-based AErosol RObotic NETwork (AERONET) have contributed immensely to quantitative characteristics of SSA in terms of AOD (the column integrated aerosol extinction), size distribution information, and spectral optical properties. Although passive instruments have been useful for developing a basic picture of SSA distribution, they supply limited information on aerosol speciation and very little data related to aerosol distribution in the vertical column. The introduction of the Cloud-Aerosol Lidar with Orthogonal Polarization (CALIOP) onboard the Cloud-Aerosol Lidar and Infrared Pathfinder

Satellite Observations (CALIPSO) platform has eliminated some of the assumptions made by the passive instruments and has provided a more complete picture of global aerosol distribution desirable by climate scientists. However, CALIOP is an elastic backscatter lidar with no molecular filtering capability and therefore requires the assumption of an extinction-to-backscatter ratio, also known as the lidar ratio, to infer extinction from attenuated backscatter measurements. Depending on the microphysical properties of the aerosol, the lidar ratio can have a wide range of values and therefore a straightforward a priori solution within some reasonable uncertainty range is generally unobtainable without various assumptions or constraints. Theoretical calculations for the lidar ratio can be performed, if the physicochemical properties and the size distribution of the particles at the different heights in the vertical column are known; although, the fulfillment of these requirements would make the lidar measurements unnecessary (Ackermann, 1998). The typical solution to this problem is to assign a vertically independent lidar ratio to aerosol retrievals that fit a specific aerosol model as outlined in Omar et al. (2009).

Since the uncertainty in the lidar ratio can significantly affect the accuracy of the aerosol extinction retrieval (see a detailed discussion below), lidar ratios have been constrained by numerous approaches. However, SSA size distribution, chemical composition and refractive index can change significantly with ocean surface wind speed (U_{10}), relative humidity (RH), temperature, salinity and chemical/biological composition of surface sea water (de Leeuw et al., 2011; Lewis and Schwartz, 2004). For this reason, large disagreement exists in the literature regarding the value of maritime aerosol lidar ratio (S_p; subscript "p" indicates particulate). For example, lidar measurements of (Ansmann et al., 2001) over the North Atlantic showed $S_p = 24 \pm 5$ sr whereas measurements using a nighttime lidar at a horizontal orientation off the northern coast of Queensland, Australia showed maritime aerosol lidar ratios as high as $S_p = 39 \pm 5$ (Young et al., 1993). Using the data from AERONET oceanic sites (Cattrall et al., 2005) derived a lidar ratio of 28 ± 5 sr, the value that compared well with literature averaged value of $S_p = 29 \pm 5$ sr (for $490 \leq \lambda \leq 550$ nm) for maritime aerosols. Passive techniques have also been used to derive the lidar ratio using an alternative definition of S_p as a function of single scattering albedo and the scattering phase function near 180° (Bréon, 2013). Using the multi-directional measurements of the solar radiation from the polarization sensitive passive radiometer POLDER, typical values for clean marine aerosol S_p were derived to be 25 sr at 532 nm (Bréon, 2013). The lidar ratio of 20 ± 6 sr (at 532 nm) was selected for the CALIOP

retrieval algorithm based on parameters measured during the Shoreline Environmental Aerosol Study (SEAS) experiment (Masonis et al., 2003; Omar et al., 2009). The SEAS experiment reports a particulate lidar ratio $S_p = 25.4 \pm 3.5$ sr at 532 nm based on the optical size measurements of sea spray aerosol and a modeled value of $S_p = 20.3$ sr (Masonis et al., 2003). Although the S_p value used in the CALIOP marine aerosol model is the same as the one derived using an average SSA size distribution measured on the beach (downwind of an offshore reef), modeling studies show a wide range of S_p values (from 10 to 90 sr) depending on particle size (Masonis et al., 2003) and wind speed (Sayer et al., 2012). Therefore, as size distribution (and chemical composition) of SSA may vary over the oceans, a constant lidar ratio used in CALIOP algorithms may lead to erroneous retrievals of AOD.

In this study, we present a new method for deriving lidar ratios for individual CALIOP retrievals of single aerosol layer columns over the ocean. To estimate S_p for a strictly defined subset of CALIPSO data we have used the Synergized Optical Depth of Aerosols (SODA) product (described in section 2.2). The S_p values are calculated as a correction to achieve the best agreement between SODA and CALIPSO sea spray AOD values. Using CALIPSO level 2 aerosol layer data for years 2007 to 2010, we have created a 3-year averaged climatology of clean marine aerosol lidar ratio over the globe. Analyses were also carried out to assess dependence of S_p values on wind speed and estimate possible error sources in our calculations. It should be noted that other lidars, such as the High Spectral Resolution Lidar (HSRL) (Eloranta, 2005; Hair et al., 2008) and Raman Lidar (Ansmann et al., 1990), are capable of measuring aerosol backscatter and extinction parameters independently and therefore do not require the lidar ratio to be prescribed (Shipley et al., 1983; Grund and Eloranta, 1991; Piironen and Eloranta, 1994; Müller et al., 2007; Amiridis et al., 2009; Tesche et al., 2009a,b; Burton et al., 2012). Other techniques like the inversion of AERONET radiometer data (Holben et al., 1998) along with Mie theory can also provide the lidar ratio (the supplementary Table S1 summarizes available methods to retrieve the lidar ratio). A more complete list can be found elsewhere (Cattrall et al., 2005; Smirnov et al., 2001). Despite this, currently CALIPSO is the only lidar that provides aerosol data at the vast spatiotemporal resolution required for global climate model comparison.

2 Instrumentation and Methods

2.1 CALIPSO satellite

The CALIPSO mission (Winker et al., 2009), launched on April 28, 2006, has been able to provide the scientific community with vertically resolved measurements of both aerosol and cloud optical properties like depolarization ratio (a measure of particle sphericity), AOD, and ice/water phase since June 2006. The CALIPSO payload includes a high-powered digital camera, an infrared radiometer, and a two-wavelength (532 and 1064 nm), near nadir, polarization sensitive, elastic backscatter lidar, CALIOP.

The level 1 data algorithms are responsible for the geolocation and range determination of the satellite and produce profiles of attenuated backscatter coefficients. Data in this work were obtained from the 5 km, level 2 operational products version 3.01. Level 2 products have undergone various processing algorithms from the Selective Iterated BoundarY Locator (SIBYL), the Scene Classification Algorithm (SCA), and the Hybrid Extinction Retrieval Algorithm (HERA) (Vaughan et al., 2004; 2009). First, SIBYL identifies layers, then the SCA identifies the type of feature (i.e., aerosol or cloud) and the subtype (i.e., aerosol type, ice/water phase), and finally, the HERA generates extinction profiles for the feature. The theoretical basis of the algorithm can be found online at www-calipso.larc.nasa.gov/resources/project_documentation.php.

The CALIPSO 5 km aerosol layer data includes many operational products of which only a few are used in this study. Among them are, the integrated attenuated backscatter and its uncertainty at 532 nm, the layer features such as number found in the column and their top and bottom altitudes and the feature classification flags.

2.2 Synergized Optical Depth of Aerosols (SODA)

CloudSat was launched in 2006 with CALIPSO and was positioned in sun-synchronous orbit as part of the A-Train satellite constellation. CloudSat and CALIPSO have paved the way for new multi-sensor data products like SODA to be developed. The main instrument on CloudSat is the Cloud Profiling Radar (CPR), a nearly nadir looking (0.16°) 94-GHz (≈ 3 mm; W-band) radar. The CPR, like CALIOP, can retrieve information on hydrometeor microphysical properties at different heights in a vertical column. The CPR signal is mostly attenuated by water vapor; however, for cloud free regions over the ocean, the CPR data can be used to retrieve AOD. A method developed by Josset et al. (2008) and later expanded by

Josset et al. (2010a) uses a combination of CALIOP and CPR measurements of the ocean surface reflectance to derive AOD. The design of SODA utilises the ratio of the ocean surface scattering cross section of the radar over the lidar to infer column optical depth for non-cloudy atmospheric columns. Since the radar signal attenuates mostly due to water vapor and the lidar signal weakens mostly due to aerosols, after the radar signal is corrected for attenuation by water vapor and oxygen, the change in the radar-to-lidar signal ratio is directly related to aerosol abundance (Josset et al., 2008; 2010a). Therefore, by using observations from two different sensors, SODA can eliminate uncertainties induced by the CALIOP aerosol extinction algorithm over oceans. SODA AODs have been shown to be in very good agreement with MODIS AOD retrievals (Josset et al., 2008). A more detailed description of the SODA technique and its application is given in Josset et al. (2008; 2010a; 2010b; 2011; and 2012). The SODA products that are used in this study include the quality assurance measure "qa_flag_aerosol" and the 532 nm AOD.

2.3 Lidar ratio definition

One of the biggest advantages of the SODA product is that it removes the dependence of the prescribed lidar ratio while still utilizing the active sensors to retrieve an AOD, thereby providing a means for independent evaluation of the lidar ratio. In the current study we use Eq. 4 from Josset et al. (2011) to estimate lidar ratio from CloudSat/CALIOP measurements of AOD values. Following Fernald et al. (1972), the particulate two-way transmittance at height Z can be written as:

$$T^2(Z) = e^{-2S_p \int_0^Z \beta_p(z)dz} \quad (1)$$

where the lidar ratio at height Z can be defined as the ratio of the particulate extinction to backscatter $\left(S_p = \frac{\sigma_p(Z)}{\beta_p(Z)}\right)$. Differentiating Eq. 1 with respect to vertical coordinate (z) gives the particulate backscatter at height Z:

$$\beta_p(Z) = -\frac{1}{2S_p T^2(Z)} \frac{dT^2(Z)}{dZ} \quad (2)$$

Since atmospheric constituents (molecules and different particle types) can interact with the lidar beam at different heights, the lidar ratio using remotely sensed data cannot be uniquely defined for a given atmospheric column. However, the lidar ratio is a particle intensive property (i.e., dependent on particle type and not on the amount). So, if we assume that there is only a single type of aerosol and it is homogeneously distributed throughout the atmospheric column and that molecular scattering is sufficiently removed by the CALIOP

level 2 algorithms, then the column lidar ratio ($\overline{S_p}$) can be expressed as the ratio of the particulate column integrated extinction ($\overline{\tau_p}$ = AOD) to the attenuated backscatter ($\overline{\Gamma_p}$). Based on these assumptions, integration of Eq. 2 with respect to vertical coordinate gives the particulate lidar ratio as:

$$\overline{S_p} = \frac{\int_{T_p^2(0)}^{T_p^2(Z)} d\,T^2(z)}{\int_0^Z \beta_p\,(z) {T_p}^2(z) dz} \tag{3}$$

If we first substitute in Eq. 3 the definition for two-way transmittance as $T_p^2 = e^{-2\overline{\tau_p}}$, then substitute the total particulate attenuated backscatter signal retrieved by the lidar as $\overline{\Gamma_p} = \int_0^Z \beta_p\,(z) T^2(z) dz$ and finally consider that $T_p^2(0) = 1$, the equation for a columnar particulate lidar ratio is:

$$\overline{S_p} = \frac{1 - e^{-2\overline{\tau_p}}}{2\overline{\Gamma_p}} \tag{4}$$

Equation 4 allows us to calculate SSA lidar ratio from two independent sources: the AOD (i.e., $\overline{\tau_p}$) from SODA and the integrated attenuated backscatter ($\overline{\Gamma_p}$) from CALIOP. It should be noted that CALIOP estimation of $\overline{\Gamma_p}$ is difficult for layers that are not bounded by clear air (Vaughan et al., 2004) and therefore require carefully designed data screening algorithms. In section 4 we carry out an error analysis to verify that uncertainties in $\overline{\Gamma_p}$ have a minimal effect on the retrieved lidar ratio.

2.4 Data selection method

As different aerosol sub-types have different lidar ratios, application of Eq. 4 to episodes when aerosols other than sea spray are present in the atmospheric column may lead to erroneous results for the calculated $\overline{S_p}$. To minimise the contamination of sea spray AOD and therefore $\overline{S_p}$ by aerosol types other than SSA (e.g., anthropogenic pollution, biomass burning, and dust), we developed a strict scene selection algorithm. The algorithm first uses the feature classification flags in the CALIOP aerosol layer product. We start with clean marine aerosol that is identified based on surface type (as determined by the location of the satellite) and either total integrated attenuated backscatter $\gamma' > 0.01$ km^{-1}sr^{-1} or total integrated attenuated backscatter $g¢< 0.01$ km^{-1}sr^{-1} and volume depolarization ratio $\delta' < 0.05$ (Omar et al., 2009). As multiple types of aerosols can be found within retrieved vertical profiles (e.g., dust above sea spray), aerosol feature types that have been identified as

marine in a given atmospheric column are not enough to carry out the analysis. Therefore, when determining the lidar ratio of SSA using Eq. 4, the algorithm only retains the data in which sea spray is the only type of aerosol present in the entire atmospheric column. To further reduce the uncertainty, we constrain the analysis to single layer profiles and remove profiles in which marine aerosol layers are vertically stacked within an atmospheric column. Therefore, the vertically integrated particulate attenuated backscatter $\overline{\Gamma_p}$ is replaced by Γ_p. Similarly, the column lidar ratio $\overline{S_p}$ is reduced to S_p for the remainder of the paper. Note also that all quantities discussed are particulate quantities and therefore, molecular scattering is removed using gridded molecular and ozone number density profile data from the Goddard Earth Observing System Model, version 5 (GEOS-5) analysis product available from the NASA Global Modeling and Assimilation Office (GMAO) (Winker et al., 2009). Operationally, particulate scattering is determined to be where the ratio of the CALIOP 532 nm scattering profile normalised by the GEOS-5 molecular scattering profile is greater than one $\left(\frac{\beta'_{532}}{\beta_m} > 1\right)$. Errors associated with $\overline{\Gamma_p}$ are discussed in Sec. 4.

In this study, CALIOP and SODA nighttime data are collected globally for a period of three years from December 2007 to February 2010. The global data are then binned into 2º × 5º latitude and longitude, respectively, grid cells. The data is binned according to season and ocean surface wind speed (taken from the Advanced Microwave Scanning Radiometer - Earth (AMSR-E) observing system). To identify distinct features associated with the variability in sea spray aerosol lidar ratio over different parts of the oceans, the selected data is examined in relationship with other variables such as season, spatial location, and wind speed.

For the data analyses conducted in this study, the single layer columns that have been identified by CALIPSO as clean marine aerosol were isolated and binned when the following conditions were met: (i) the vertical feature mask found 1 layer in the entire column, (ii) the vertical feature mask ranked the layer as type: *aerosol* and subtype: *clean marine*, (iii) the layer top was $<$ 2 km, (iv) the relative error in Γ_p due to random noise in molecular backscatter was $<$ 50%, (v) the collocated SODA 5 km layer was composed of at least 70% shot-to-shot data (therefore increasing the signal to noise ratio), (vi) the total number of retrievals per 2º × 5º grid cell ranked above the first quartile of the grid cell frequency distribution (i.e., grid cells with frequency data in the lower 25% of the distribution have not been included in the data analysis and are masked in the subsequent figures), and (vii) only nighttime data was used. Such strict quality controls, although reducing the total number of

data points, considerably increase the reliability of the selected episodes. It should be noted that even after all the quality control and quality assurance tests have been conducted, a large number (over 260,000) of data points allowed a robust statistical analysis to be conducted.

To further minimise the effect of outliers on the estimated value, statistical medians were calculated for each grid cell. Regions where grid cells fail criteria (vi) indicate low confidence in the reported median value due to a low number of observations and are removed. This also ensures that global means are not heavily biased by outliers resulting from grid cells with a low number of retrievals. This procedure allows the removal of the non-physical positive skewness of the distribution observed by Josset et al. (2012). Despite such rigorous quality control criteria, readers should be cautioned when interpreting data near coastlines as the CALIOP scene classification algorithm may mistakenly identify mixtures of continental pollution and marine as clean marine aerosol (Burton et al., 2013; Oo and Holz, 2011; Schuster et al., 2012) causing an overestimation in the lidar ratio inferred from Eq. 4. Further discussion of error analysis is given in Sec. 4 below.

3 Results

3.1 Global distribution of retrieved AOD and lidar ratio

Active detectors like CALIOP require knowledge of the lidar ratio for retrieval of aerosol optical properties. Incorrect estimates of the S_p values for a given aerosol type can lead to significant errors in the retrievals of particulate extinction and AOD. Past studies using collocated CALIOP and MODIS retrievals have shown that, over the marine regions, CALIOP underestimates the AOD values relative to MODIS (Oo and Holz, 2011). As MODIS data over the ocean has been extensively evaluated with numerous field campaigns (e.g., Levy et al., 2005), it was suggested that the primary source of discrepancy between the two sensors was the low value of the SSA lidar ratio used by CALIOP (Oo and Holz, 2011). Figure 1 shows seasonally averaged maps of CALIPSO and SODA SSA median optical depth at 532 nm and the differences between SODA and CALIOP retrieved AODs. White regions on Fig. 1 represent grid cells that were rejected by the data selection algorithm and have been removed from the subsequent data analysis. Inspection of Fig. 1 reveals considerable spatial and temporal variations in sea spray AOD. Although the largest values of AOD seem to occur over regions with higher surface wind speed (i.e., the northern and southern oceans), elevated AOD values can also be seen over the regions downwind from dust and/or pollution sources such as the mid-latitude North Atlantic Ocean and the Bay of

Bengal and over the major oceanic gyres. The region around the Indian subcontinent and over the Bay of Bengal is believed to be just a retrieval artifact. Large disagreements between SODA and CALIOP reported AODs for these regions suggest that some dust/pollution aerosols might have been misclassified by CALIOP as sea spray. Higher S_p values for dust and pollution compared to SSA would produce a higher AOD retrieval in SODA compared to CALIOP. Elevated AOD values over the oceanic regions with lower surface wind speed, on the other hand, could point to changes in sea spray particle size distribution to smaller sizes. Sub-micron sea salt aerosols (with particle diameter, D_p< 1 μm) are believed to have larger lidar ratios than super-micron ones (e.g., Masonis et al., 2003; Oo and Holz, 2011). In general, Fig. 1 shows positive differences between SODA and CALIOP retrieved seasonal median AOD values. Recalling that CALIOP retrieved extinction is the product of the prescribed lidar ratio and the measured column integrated particulate backscatter, positive differences between SODA and CALIOP median AODs at 532 nm over most of the oceans suggest underestimation of the SSA lidar ratio prescribed in the CALIOP clean marine aerosol model. Figure 2 shows that over most of the ocean surfaces, the calculated lidar ratio is higher than the default (S_p = 20 sr) used in the CALIOP clean marine aerosol model. Global means and standard deviations for AOD and lidar ratio are given in Table 1. CALIOP retrievals in this study cannot be directly compared to MODIS since we only use nighttime data. Nevertheless, SODA retrievals of AOD have been shown to agree well with MODIS (Josset et al., 2008) suggesting that the corrected lidar ratios will bring CALIOP retrievals close to MODIS data. Figure 2 also reveals that the value of the lidar ratio calculated using Eq. 4 changes considerably over different parts of the remote oceans, pointing to the variability in sea spray aerosol optical properties. It has long been known that meteorological and/or environmental factors and ocean chemical/biological composition influence SSA production, entrainment, transport, and removal processes (Lewis and Schwartz, 2004) that can ultimately affect S_p. Moreover, due to atmospheric transport of SSA, satellite retrieved AOD values may also be related to the upwind processes. Despite the complexity of the mechanisms controlling SSA mass concentration over the oceans, surface wind speed has always been considered as the major parameter governing the production, chemical composition, and life cycle of SSA (Lewis and Schwartz, 2004). Therefore, in the next section we will investigate the effect of wind speed on calculated temporal variability of marine aerosol lidar ratio.

3.2 Wind speed dependence

Numerous investigators have examined the effect of sea surface wind speed and sea state on marine aerosol optical properties (e.g., Smirnov et al., 2003; Sayer et al., 2012). There are two production mechanisms for sea spray particles: bursting of bubbles at the water surface, and mechanical tearing of water drops (spume) from wave crests (for surface wind speeds $U_{10} > 9$ ms^{-1}, Anguelova et al., 1999). Ocean bubbles are generated by the entrainment of air due to wave action. As bubbles rise due to their buoyancy, they burst at the surface producing SSA (Blanchard and Woodcock, 1957). In this study we have selected seven different wind speed regimes (see Table 2). The lowest wind speed regime, $0 < U_{10} \leq 4$ ms^{-1}, was chosen to represent aerosols not generated via wind driven processes over the ocean. In general, ocean waves break at wind speed values above ~ 4 ms^{-1} (initiating the white cap formation and bursting of the entrained bubbles) (Lewis and Schwartz, 2004). Therefore, it has been suggested that below this threshold value, there should be a weak relationship between SSA optical properties and the surface wind speed (Kiliyanpilakkil and Meskhidze, 2011; Lehahn et al., 2010). Moreover, for such a low wind speed regime, most of the aerosols classified as clean marine by CALIOP are either produced outside the swath and then blown into the satellite field of view, or like in cases near coastlines, mistakenly identified as SSA. The highest wind speed regime, with U_{10} > 15 ms^{-1}, typically contributes a small fraction of CALIOP retrievals (Kiliyanpilakkil and Meskhidze, 2011) and is largely concentrated over the southern ocean and in the northern Atlantic where the highest wind speeds are observed (Bentamy et al., 2003). Although CALIOP retrieval counts for sea spray aerosol in each 2º × 5º grid cell are also influenced by the presence of clouds, Fig. S1 shows the global distributions of CALIOP retrieval frequencies for different wind speed regimes. Figure 3 shows the scatterplots for SODA and CALIOP retrieved AOD values for the wind speed regimes of Table 2. As expected, Fig. 3 shows that increases in wind speed are typically associated with higher values of SSA optical depth (note the center of the scatter distribution shifts to higher AODs for larger wind speed values). However, as the majority of the SODA AODs exist above the 1:1 line, this figure also indicates the underestimation of CALIOP retrieved SSA optical depth values. When averaged over the entire globe, CALIOP retrieved clean marine AOD is roughly 32% lower compared to SODA. According to Fig. 3 the largest discrepancies between SODA and CALIOP retrievals are observed at lower wind speed values. One easy explanation for this is greater chance for CALIOP misclassification over the oceanic regions where long-ranged continental aerosols can contribute a larger fraction of the

MBL particles (e.g., Blot et al., 2013). Terrestrial particles (e.g., mineral dust, anthropogenic pollution) are typically characterised by the larger lidar ratio values, leading to underestimation of the CALIOP retrieved AODs. However, measurements also show that changes in surface wind speed values can cause a considerable shift in the SSA size distribution. For optically active sea spray particles, the residence time decreases considerably with increasing size. Thus the aerosol population is increasingly controlled by the smaller end of the particle size spectrum as wind speeds decrease over the ocean (Hoffman and Duce, 1974). Conversely, as wind speed increases, fine mode aerosol volume size distribution changes slightly (with mixed trends), while the coarse mode volume size distribution exhibits a large and positive response to the increase in wind speed (Lewis and Schwartz, 2004; Smirnov et al., 2003). Such variability in SSA volume size distribution is expected to have an effect on the aerosol lidar ratio. As sub-micron sea salt aerosols are characterised with much larger lidar ratios than super-micron ones (e.g., Masonis et al., 2003; Oo and Holz, 2011), shifting SSA size distribution spectra to smaller particles will cause an increase in total aerosol lidar ratio. Therefore, for clean marine aerosols, AODs and lidar ratios are expected to have opposite dependences on wind speed: high wind speed regions are characteristic of high AODs and low lidar ratios while lower wind speeds favor higher lidar ratios and lower AODs (Smirnov et al. 2003; Sayer et al., 2012).

Figure 4 shows that on average, the calculated aerosol lidar ratio is inversely related to the surface wind speed. According to this figure, aerosols retrieved in the wind speed regime $0 < U_{10} \leq 4$ ms^{-1} depict the largest variability in the lidar ratio as indicated by the spread of the distribution. As discussed above, aerosols in this regime likely include both sea spray particles produced upwind and advected into the satellite field of view (with S_p ~ 20 to 30 sr), as well as dust/pollution particles (with S_p ~ 40 to 70 sr, Omar et al., 2009) that may have been misclassified by CALIOP as sea spray. As shown in Table 2, SSA lidar ratio distribution in this regime is characterised by the largest standard deviation ($\sigma = 17.4$ sr) indicating that for the lowest wind speed values, a wide range of sea spray particle sizes can be present over the ocean. Since for the wind speed values less than 4 m s^{-1}, the sea spray production is minimal, such large spread could also indicate that under low wind conditions there is greater probability for natural continental and human-induced pollution aerosols be miss-classified by CALIOP as clean marine.

For the higher wind speed values ($4 < U_{10} \leq 15$ ms^{-1}) lidar ratio generally decreases with the increase in the wind speed and approaches the lidar ratios prescribed by CALIOP

retrieval algorithms (i.e., 20 sr) at the highest wind speed regime. According to Fig. S1, the most common wind values in CALIOP SSA retrievals over the ocean are in the $8 < U_{10} \leq 10$ ms^{-1} regime (26% of all available data) followed by the $6 < U_{10} \leq 8$ ms^{-1} regime (23% of all available data). For the higher wind speed regimes ($U_{10} \gtrsim 6\ \mathrm{ms}^{-1}$), surface winds play a decisive role in the determination of the lidar ratio (indicated by the narrow standard deviation, see Table 2). This is an important result as the distributions shown on Fig. 4 may help providing additional criteria for clean marine lidar ratio selection, yielding improved retrieval of sea spray AOD from CALIOP.

Analysis of data indicates that a mean lidar ratio of 26 sr is the most probable value that occurs for the majority of CALIOP retrievals over the oceans. This new lidar ratio reduces discrepancy between CALIOP-prescribed and SODA-derived lidar ratios from about 30% to 4%. Although the mean S_p = 26 sr value for SSA proposed in this study considerably improves relationship between SODA and CALIOP retrievals for a wide range of ocean surface wind speed values, the added advantage of the current analysis is the ability to correct individual CALIOP retrievals of sea spray AODs. The correction to the lidar ratio can be prescribed using Eq. 4 as:

$$1 - e^{-2\tau_S} = \frac{S_{p,S}}{S_{p,C}}(1 - e^{-2\tau_C}) \qquad (5)$$

where the subscripts *C* and *S* stand for CALIOP default ($S_{p,C}$) and suggested ($S_{p,S}$) lidar ratios, respectively. In future studies we intend to examine a limited number of parameters (in addition to wind speed) to construct a look-up table with a wind speed dependent, spatiotemporal distributions of SSA lidar ratios for use in CALIOP clean marine aerosol retrievals.

In the meantime, however, we have provided a parameterization of the lidar ratio with wind speed in the supplementary information (Fig. S2), as this is of interest to the sea spray community. We have considered a full range of wind speeds from 0 - 25 ms^{-1} in our parameterization, but given the low number of retrievals at very low ($<4\,\mathrm{ms}^{-1}$) and very high ($>15\,\mathrm{ms}^{-1}$) wind speeds, along with the large range of lidar ratios retrieved at low wind speeds (roughly ± 17 sr), we recognize the need for further constraints in these regions. Considering the number of retrievals and confidence bounds, we believe our parameterization is a useful tool for predicting sea spray aerosol S_p ($\lambda = 532$ nm) at wind speeds between 8 and 15 ms^{-1} with an error of ± 2 sr.

4 Assessing the validity and sensitivity of Γ_p

The method used to derive the lidar ratio in this study depends on two parameters: the CALIOP integrated attenuated particulate backscatter (Γ_p) and the SODA aerosol optical depth (τ_p). Uncertainties in both Γ_p and τ_p retrievals are expected to propagate through the calculations of the particulate lidar ratio. Josset et al. (2008; 2010a) investigate the domain of validity for τ_p through an extensive calibration procedure. They find that for retrievals at wind speeds between 3 and 10 ms^{-1} the SODA product is in very good agreement $(R > 0.89)$ with MODIS AOD with calibration errors less than 15%. Calibration errors in τ_p are expected to be even lower for nighttime retrievals used in this study (Josset et al. 2008). On the other hand, average uncertainty for CALIOP Γ_p retrievals has not been examined previously and will be determined below.

Since ocean is the source of SSA, clean marine aerosol layers typically extend to the ocean surface. This makes it more difficult to determine molecular and particulate backscatter components of the signal separately using satellite measurements alone. To assess the uncertainty in lidar ratio introduced for the surface connected layers (i.e., layers whose bottom bound is defined as the ocean surface), here we estimate the error in CALIOP retrieved Γ_p values. The total attenuated backscatter signal measured by the lidar consists of molecular and particulate components:

$$\beta_{att} = (\beta_p + \beta_m)\, e^{-2\tau_p} \cdot e^{-2\tau_m} \tag{6}$$

with subscripts *m* and *p* representing molecular and particulate quantities, respectively. From the definition of Γ_p it follows that:

$$\Gamma_p = \int_0^Z \beta_p(z)\, e^{-2\tau_p}\, dz \tag{7}$$

where the integration is from the surface to the top of the layer. β_p is the particulate backscatter and $e^{-2\tau_p}$ accounts for the attenuation of the lidar signal by the particles. Substituting Eq. 6 into Eq. 7 gives:

$$\Gamma_p = \int_0^Z (\beta_{att}\, e^{2\tau_m} - \beta_m(z) e^{-2\tau_p}) dz \tag{8}$$

The molecular component of the signal in Eq. 8 can be derived from the GMAO modeled temperature and pressure profiles (Bloom et al., 2005). However, to solve this equation and determine the particulate attenuated backscatter value, particulate column integrated extinction is required. To get τ_p the CALIOP algorithm is using a prescribed value of the lidar ratio, making Eq. 4 circularly dependent on the lidar ratio. The error in CALIOP retrieved Γ_p associated with the prescribed lidar ratio can be estimated by substituting the

τ_p value from SODA. If the error is large, that would imply that the uncertainty in CALIOP prescribed lidar ratio would introduce sizable corrections to Γ_p, making Eq. 4 unsuitable for the estimation of SSA lidar ratio.

The relative error in Γ_p can be defined as:

$$Error = \frac{\Gamma_{p,S} - \Gamma_{p,C}}{\Gamma_{p,C}} = \frac{(e^{-2\tau_{p,C}} - e^{-2\tau_{p,S}}) \cdot \int_0^Z \beta_m(z)dz}{\Gamma_{p,C}} \quad (9)$$

where $\Gamma_{p,S}$ and $\Gamma_{p,C}$ are columnar integrated attenuated backscatter values for SODA and CALIOP, respectively. From the theoretical basis documents for CALIOP level 1 algorithms, the molecular backscatter is estimated as $\beta_m = \frac{C_s}{S_m}\frac{T(z)}{P(z)}$ where height dependent *T(z)* and *P(z)* profiles from the surface (1000 hPa) to top-of-atmosphere (0.1 hPa) pressure levels were obtained from the GMAO Modern-Era Retrospective analysis for Research and Applications dataset. The molecular lidar ratio, S_m is defined as $8\pi/3$ and C_s is a constant equal to 3.742×10^{-6} K/hPa/m (Hostetler et al., 2005). When considering all of the parameters, our analysis shows that the average error in Γ_p is approximately 1.5%. Compared to the systematic uncertainty in the SODA product ($< 15\%$), the uncertainty in Γ_p is much lower indicating that, on average, errors in Γ_p do not dominate S_p retrievals. Since an average discrepancy between CALIOP-prescribed and SODA-derived lidar ratios (~30%) is more than an order of magnitude higher than uncertainty in Γ_p, we conclude that the uncertainty in the CALIOP column integrated backscatter has a minor effect on the Eq. 4 calculated lidar ratio.

Furthermore, because in our study we use feature integrated products for a single aerosol layer, it is also important to evaluate the relationship between Γ_p and aerosol layer thickness (ΔZ). Figure 5 shows the normalised column attenuated particulate backscatter Γ_p as a function of layer depth. For uniformly distributed aerosols throughout the column, Γ_p is likely to be proportional to ΔZ. The spread of $\Gamma_p/\Delta Z$ ratio is indicative of different amounts of SSA present in the column. Two limits of very high and very low ΔZ values are of particular interest. For example, strong reduction of the $\Gamma_p/\Delta Z$ ratio at the higher ΔZ values would indicate that the lidar signal is strongly attenuated throughout the layer reaching a sensitivity limit. On the other hand, considerable increase of the ratio for the thin layers may indicate contamination of the backscattered signal by the surface reflectance. According to Fig. 5 for the vast majority of the data, signal attenuation and surface reflectance do not seem to be major issues for the surface connected layers, suggesting that the quality control

algorithm described in Sec. 2.4 was sufficient to remove the majority of erroneous measures of Γ_p.

5 Conclusions

A new method showing that it is possible to infer lidar ratios of sea spray aerosol over the ocean using two independent sources: the AOD from Synergized Optical Depth of Aerosols (SODA) and the integrated attenuated backscatter from Cloud-Aerosol Lidar with Orthogonal Polarization (CALIOP) has here been applied. The proposed equation calculates particulate lidar ratio for individual CALIOP retrievals of single aerosol layer columns as a correction to achieve the best agreement between SODA and CALIOP retrievals. The new method allows calculating sea spray lidar ratio and assessing its spatiotemporal variability and dependence on ocean surface wind speed. Analyses were carried out using CALIOP level 2, 5km aerosol layer and collocated SODA nighttime data from December 2007 to February 2010. During the data analysis over 260,000 data points passed various quality-control and quality-assurance tests to reduce errors associated with the clean marine aerosol retrievals. The calculated lidar ratios have been analyzed over the global ocean covering a wide range of wind speed and AOD conditions. Data analysis shows that over most of the ocean surfaces, the calculated lidar ratio is higher than the default lidar ratio of 20 sr used in the CALIOP clean marine aerosol model. The calculated aerosol lidar ratios are inversely related to the surface wind speed. Increases in mean surface ocean wind speeds from 0 to >15 ms^{-1} reduces the mean lidar ratio for sea spray particles from ~32 sr to ~22 sr. Such reduction was explained by the shift in aerosol volume size distribution with the wind speed; however, it was also emphasised that future studies should explore the role of meteorological and/or environmental factors and ocean chemical/biological composition for sea spray aerosol intensive properties. Our data analysis showed that changes in wind speed also affect the probability density function for sea spray aerosol (SSA) lidar ratio distribution. The largest standard deviation calculated for the lowest wind speed regime suggested that under low wind conditions, a wide range of sea spray particle sizes can be present over the ocean and there is greater probability for natural-continental and human-induced pollution aerosols to be classified by CALIOP as clean marine. We would like to mention that the role of organic aerosol at low wind speeds is still unclear. A large body of experimental data suggests that increases in the organic fraction of marine aerosol can have implications on hygroscopicity (e.g. Saxena et al., 1995; Fuentes et al., 2011; Ovadenevaite et al., 2013) and could

potentially influence our results. Overall, our data analysis shows that an average value of 26 sr for SSA lidar ratio provides the best agreement between the SODA product and CALIOP retrieved global mean sea spray aerosol optical depth values. However, our study also shows large spatiotemporal variability in SSA lidar ratios, suggesting that a single constant value of the lidar ratio is not suitable for a wide range of sea spray aerosols and can lead to large uncertainties at different locations and seasons.

We have estimated the error in CALIOP retrieved column integrated attenuated particulate backscatter. Calculations suggest that the average uncertainty in particulate backscatter is more than an order of magnitude lower compared to the retrieved value. Data analysis also showed no clear indication for either approaching a sensitivity limit (due to strong attenuation of the lidar signal throughout the layer) or the contamination of the backscattered signal by the surface reflectance. Based on the conducted error analysis we conclude that the strict quality control criteria developed in this study is adequate to remove the majority of erroneous retrievals.

Finally, even though calculations here were carried out for SSA, the technique used in this study is broad and can be used to infer lidar ratios of different species of atmospheric aerosols (i.e., mineral dust, biomass burning, etc.) advecting over the ocean. Because our data analysis shows that it is possible to derive a correction to the CALIOP prescribed sea spray lidar ratio, future studies should also consider conducting case studies over different oceanic regions to examine the possible effects of meteorological parameters and ocean physiochemical/biological composition on sea spray aerosol lidar ratio. Classification (in the form of a look-up table) of spatiotemporal distribution and wind speed dependence of a limited number of parameters mostly affecting SSA lidar ratios, may lead to improved retrievals of AOD values over the oceans.

Acknowledgements

This research was supported by the National Aeronautics & Space Administration (NASA) through grant no NNX11AG72G and by the National Science Foundation through the grant AGS-1249273. The authors gratefully acknowledge the CALIPSO and CloudSat Teams for their effort in making the data available. CALIPSO data were obtained from the NASA Langley Research Center Atmospheric Science Data Center. CloudSat data are produced by Remote Sensing Systems and sponsored by the NASA Earth Science MEaSUREs DISCOVER Project and the Advanced Microwave Scanning Radiometer (AMSR-E) Science

Team. The SODA product is developed at the ICARE data and services center (http://www.icare.univ-lille1.fr) in Lille (France) in the frame of the CALIPSO mission and supported by CNES.

References

Ackermann, J.: The extinction-to-backscatter ratio of tropospheric aerosol: A numerical study, J. Atmos. Ocean. Technol., 15, 1043-1050, doi: 10.1175/1520-0426(1998)015<1043:TETBRO>2.0.CO;2, 1998.

Amiridis, V., Balis, D. S., Giannakaki, E., Stohl, A., Kazadzis, S., Koukouli, M. E. and Zanis, P.: Optical characteristics of biomass burning aerosols over Southeastern Europe determined from UV-Raman lidar measurements, Atmos. Chem. and Phys., 9, 2431-2440, doi:10.5194/acp-9-2431-2009, 2009.

Andreae, M. O.: Aerosols before Pollution, Science, 315, 50-51, 10.2307/20035138, 2007.

Anguelova, M., Barber Jr, R. P. and Wu, J.: Spume drops produced by the wind tearing of wave crests, J. Phys. Oceanogr., 29, 1156-1165, doi:10.1175/1520-0485(1999)0292.0.CO;2, 1999.

Ansmann, A., Riebesell, M. and Weitkamp, C.: Measurement of atmospheric aerosol extinction profiles with a Raman lidar, Opt. Lett., 15, 746-748, doi:10.1364/OL.15.000746, 1990.

Ansmann, A., Wagner, F., Althausen, D., Müller, D., Herber, A. and Wandinger, U.: European pollution outbreaks during ACE 2: Lofted aerosol plumes observed with Raman lidar at the Portuguese coast, J. Geophys. Res., 106, 20725-20,733, doi:10.1029/2000JD000091, 2001.

Ansmann, A. and Múller, D.: Lidar and Atmospheric Aerosol Particles, in: Lidar, Weitkamp, C. (Ed.), Springer New York, 105-141, 2005.

Bentamy, A., Katsaros, K. B., Mestas-Nuñez, A. M., Drennan, W. M., Forde, E. B. and Roquet, H.: Satellite estimates of wind speed and latent heat flux over the global oceans, J. Clim., 16, 637-656, doi:10.1175/1520-0442(2003)016<0637:SEOWSA>2.0.CO;2, 2003.

Blanchard, D. and Woodcock, A.: Bubble formation and modification in the sea and its meteorological significance, Tellus, 9, 145-158, doi: 10.1111/j.2153-3490.1957.tb01867.x, 1957.

Bloom, S., Da Silva, A., Dee, D., Bosilovich, M., Chern, J., Pawson, S., Schubert, S., Sienkiewicz, M., Stajner, I. and Tan, W.: Documentation and validation of the Goddard Earth Observing System (GEOS) data assimilation system–Version 4, NASA Tech. Memo., 104606, 187, 2005.

Blot, R., Clarke, A. D., Freitag, S., Kapustin, V., Howell, S. G., Jensen, J. B., Shank, L. M., McNaughton, C. S. and Brekhovskikh, V.: Ultrafine sea spray aerosol over the southeastern Pacific: open-ocean contributions to marine boundary layer CCN, Atmos. Chem. Phys., 13, 7263-7278, doi:10.5194/acp-13-7263-2013, 2013.

Bréon, F. M.: Aerosol extinction-to-backscatter ratio derived from passive satellite measurements, Atmos. Chem. Phys., 13, 8947-8954, doi:10.5194/acp-13-8947-2013, 2013.

Burton, S., Ferrare, R., Hostetler, C., Hair, J., Rogers, R., Obland, M., Butler, C., Cook, A., Harper, D. and Froyd, K.: Aerosol classification using airborne High Spectral Resolution Lidar measurements–methodology and examples, Atmos. Meas. Tech., 5, 73-98, doi:10.5194/amtd-4-5631-2011, 2012.

Burton, S. P., Ferrare, R. A., Vaughan, M. A., Omar, A. H., Rogers, R. R., Hostetler, C. A., and Hair, J. W.: Aerosol classification from airborne HSRL and comparisons with the CALIPSO vertical feature mask, Atmos. Meas. Tech., 6, 1397-1412, doi:10.5194/amt-6-1397-2013, 2013.

Carslaw, K. S., Lee, L. A., Reddington, C. L., Pringle, K. J., Rap, A., Forster, P. M., Mann, G. W., Spracklen, D. V., Woodhouse, M. T., Regayre, L. A. and Pierce, J. R.: Large contribution of natural aerosols to uncertainty in indirect forcing, Nature, 503, 67, doi:10.1038/nature12674.

Cattrall, C., Reagan, J., Thome, K. and Dubovik, O.: Variability of aerosol and spectral lidar and backscatter and extinction ratios of key aerosol types derived from selected Aerosol Robotic Network locations, J. Geophys. Res., 110, D10S11, doi:10.1029/2004JD005124, 2005.

de Leeuw, G., Andreas, E. L., Anguelova, M. D., Fairall, C., Lewis, E. R., O'Dowd, C., Schulz, M. and Schwartz, S. E.: Production flux of sea spray aerosol, Rev. Geophys., 49, doi:10.1029/2010RG000349, 2011.

Eloranta, E.: High spectral resolution lidar, in: Lidar: Range-Resolved Optical Remote Sensing of the Atmosphere, edited by: Weitkamp, K., Springer, New York, 143-163, 2005.

Fernald, F. G., Herman, B. M. and Reagan, J. A.: Determination of aerosol height distributions by lidar, J. Appl. Meteorol., 11, 482-489, 1972.

Fuentes, E., Coe, H., Green, D. and McFiggans, G.: On the impacts of phytoplankton-derived organic matter on the properties of the primary marine aerosol - Part 2: Composition, hygroscopicity and cloud condensation activity, Atmos. Chem. Phys., 11, 2585-2602, doi:10.5194/acp-11-2585-2011, 2011.

Ghan, S., Laulainen, N., Easter, R., Wagener, R., Nemesure, S., Chapman, E., Zhang, Y. and Leung, R.: Evaluation of aerosol direct radiative forcing in MIRAGE, J. Geophys. Res., 106, 5295-5316, doi:10.1029/2000JD900502, 2001.

Groß S., Esselborn, M., Weinzierl, B., Wirth, M., Fix, A. and Petzold, A.: Aerosol classification by airborne high spectral resolution lidar observations, Atmos. Chem. Phys., 13, 2487-2505, doi:10.5194/acp-13-2487-2013, 2013.

Groß, S., Gasteiger, J., Freudenthaler, V., Wiegner, M., Geiß, A., Schladitz, A., Toledano, C., Kandler, K., Tesche, M., Ansmann, A. and Wiedensohler, A.: Characterization of the planetary boundary layer during SAMUM-2 by means of lidar measurements, Tellus B, 63, 695-705, doi:10.1111/j.1600-0889.2011.00557.x, 2011a.

Groß S., Tesche, M., Voker, F., Toledano, C., Wiegner, M., Ansmann, A., Althausen, D., Seefeldner,M.: Characterization of Saharan dust, marine aerosols and mixtures of

biomass-burning aerosols and dust by means of multi-wavelength depolarization and Raman lidar measurements during SAMUM 2, Tellus B, 63, 706-724, doi:10.1111/j.1600-0889.2011.00556.x, 2011b.

Grund, C. J. and Eloranta, E. W.: University of Wisconsin High Spectral Resolution Lidar, Optical Engineering, 30, 6-12, doi:10.1117/12.55766, 1991.

Hair, J. W., Hostetler, C. A., Cook, A. L., Harper, D. B., Ferrare, R. A., Mack, T. L., Welch, W., Izquierdo, L. R. and Hovis, F. E.: Airborne High Spectral Resolution Lidar for profiling aerosol optical properties, Appl. Opt., 47, 6734-6752, doi:10.1364/AO.47.006734, 2008.

Hoffman, E. J. and Duce, R. A.: The organic carbon content of marine aerosols collected on Bermuda, J. Geophys. Res., 79, 4474-4477, 1974.

Holben, B. N., Eck, T. F., Slutsker, I., Tanré, D., Buis, J. P., Setzer, A., Vermote, E., Reagan, J. A., Kaufman, Y. J., Nakajima, T., Lavenu, F., Jankowiak, I. and Smirnov, A.: AERONET-A Federated Instrument Network and Data Archive for Aerosol Characterization, Remote Sens. Environ., 66, 1, doi:10.1016/S0034-4257(98)00031-5, 1998.

Hoose, C., Kristjánsson, J., Iversen, T., Kirkevåg, A., Seland, Ø and Gettelman, A.: Constraining cloud droplet number concentration in GCMs suppresses the aerosol indirect effect, Geophys. Res. Lett., 36, L12807, doi:10.1029/2009GL038568, 2009.

Hostetler, C., Liu, Z., Reagan, J., Vaughan, M., Winker, D., Osborn, M., Hunt, W., Powell, K. and Trepte, C.: CALIOP algorithm theoretical basis document–Part 1: Lidar level I ATBD-Calibration and level 1 data products, Rep.PC-SCI, 201, 66, 2005.

Josset, D., Pelon, J., Protat, A. and Flamant, C.: New approach to determine aerosol optical depth from combined CALIPSO and CloudSat ocean surface echoes, Geophys. Res. Lett., 35, L10805, doi:10.1029/2008GL033442, 2008.

Josset, D., Pelon, J. and Hu, Y.: Multi-instrument calibration method based on a multiwavelength ocean surface model, Geoscience and Remote Sensing Letters, IEEE, 7, 195-199, doi:10.1109/LGRS.2009.2030906, 2010a.

Josset, D., Zhai, P., Hu, Y., Pelon, J. and Lucker, P. L.: Lidar equation for ocean surface and subsurface, Opt. Express, 18, 20862-20875, doi:10.1364/OE.18.020862, 2010b.

Josset, D., Rogers, R., Pelon, J., Hu, Y., Liu, Z., Omar, A. and Zhai, P.: CALIPSO lidar ratio retrieval over the ocean, Opt. Express, 19, 18696-18706, doi:10.1364/OE.19.018696, 2011.

Josset, D., Pelon, J., Garnier, A., Hu, Y., Vaughan, M., Zhai, P., Kuehn, R. and Lucker, P.: Cirrus optical depth and lidar ratio retrieval from combined CALIPSO-CloudSat observations using ocean surface echo, J. Geophys. Res., 117, D05207, doi:10.1029/2011JD016959, 2012.

Kaufman, Y. J., Tanré, D. and Boucher, O.: A satellite view of aerosols in the climate system, Nature, 419, 215-223, doi:10.1038/nature01091, 2002.

Kiliyanpilakkil, V. P. and Meskhidze, N.: Deriving the effect of wind speed on clean marine aerosol optical properties using the A-Train satellites, Atmos. Chem. Phys., 11, 11401-11413, doi:10.5194/acp-11-11401-2011, 2011.

Lehahn, Y., Koren, I., Boss, E., Ben-Ami, Y. and Altaratz, O.: Estimating the maritime component of aerosol optical depth and its dependency on surface wind speed using satellite data, Atmos. Chem. Phys., 10, 6711-6720, doi:10.5194/acp-10-6711-2010, 2010.

Levy, R., Remer, L., Martins, J., Kaufman, Y., Plana-Fattori, A., Redemann, J. and Wenny, B.: Evaluation of the MODIS aerosol retrievals over ocean and land during CLAMS, J. Atmos. Sci., 62, 974-992, doi:10.1175/JAS3391.1, 2005.

Lewis, R. and Schwartz, E.: Sea salt aerosol production: mechanisms, methods, measurements and models—a critical review, American Geophysical Union, doi:10.1029/GM152, 2004.

Masonis, S. J., Anderson, T. L., Covert, D. S., Kapustin, V., Clarke, A. D., Howell, S. and Moore, K.: A Study of the Extinction-to-Backscatter Ratio of Marine Aerosol during the Shoreline Environment Aerosol Study, J. Atmos. Ocean. Technol., 20, 1388-1402, doi:10.1175/1520-0426(2003)020<1388:ASOTER>2.0.CO;2, 2003.

Meskhidze, N., Xu, J., Gantt, B., Zhang, Y., Nenes, A., Ghan, S., Liu, X., Easter, R. and Zaveri, R.: Global distribution and climate forcing of marine organic aerosol–Part 1: Model improvements and evaluation, Atmos. Chem. Phys., 11, 11689-11705, doi:10.5194/acp-11-11689-2011, 2011.

Müller, D., Ansmann, A., Mattis, I., Tesche, M., Wandinger, U., Althausen, D. and Pisani, G.: Aerosol-type-dependent lidar ratios observed with Raman lidar, J. Geophys. Res., 112, 10.1029/2006JD008292, 2007.

Omar, A. H., Winker, D. M., Kittaka, C., Vaughan, M. A., Liu, Z., Hu, Y., Trepte, C. R., Rogers, R. R., Ferrare, R. A., Lee, K., Kuehn, R. E. and Hostetler, C. A.: The CALIPSO Automated Aerosol Classification and Lidar Ratio Selection Algorithm, J. Atmos. Ocean. Technol., 26, 1994-2014, doi:10.1175/2009JTECHA1231.1, 2009.

Oo, M. and Holz, R.: Improving the CALIOP aerosol optical depth using combined MODIS-CALIOP observations and CALIOP integrated attenuated total color ratio, J. Geophys. Res., 116, D14201, doi:10.1029/2010JD014894, 2011.

Ovadnevaite, J., Ceburnis, D., Martucci, G., Bialek, J., Monahan, C., Rinaldi, M., Facchini, M. C., Berresheim, H., Worsnop, D. R. and O'Dowd, C.: Primary marine organic aerosol: A dichotomy of low hygroscopicity and high CCN activity, Geophys. Res. Lett., 38, doi:10.1029/2011GL048869, 2011.

Saxena, P., Hildemann, L. M., McMurry, P. H. and Seinfeld, J. H.: Organics alter hygroscopic behavior of atmospheric particles, J. Geophys. Res., 100, 18755-18770, doi:10.1029/95JD01835, 1995.

Sayer, A., Smirnov, A., Hsu, N. and Holben, B.: A pure marine aerosol model, for use in remote sensing applications, J. Geophys. Res., 117, doi:10.1029/2011JD016689, 2012.

Schuster, G. L., Vaughan, M., MacDonnell, D., Su, W., Winker, D., Dubovik, O., Lapyonok, T. and Trepte, C.: Comparison of CALIPSO aerosol optical depth retrievals to AERONET measurements, and a climatology for the lidar ratio of dust, Atmos. Chem. Phys., 12, 7431-7452, doi:10.5194/acp-12-7431-2012, 2012

Smirnov, A., Holben, B., Eck, T., Dubovik, O. and Slutsker, I.: Effect of wind speed on columnar aerosol optical properties at Midway Island, J. Geophys. Res., 108(D24), 4802, doi:10.1029/2003JD003879, 2003.

Tesche, M., Ansmann, A., Müller, D., Althausen, D., Engelmann, R., Freudenthaler, V. and Groß, S.: Vertically resolved separation of dust and smoke over Cape Verde using multiwavelength Raman and polarization lidars during Saharan Mineral Dust Experiment 2008, J. Geophys. Res., 114, n/a-n/a, doi:10.1029/2009JD011862, 2009a.

Tesche, M., Ansmann, A., Müller, D., Althausen, D., Mattis, I., Heese, B., Freudenthaler, V., Wiegner, M., Esselborn, M., Pisani,G., and Knippertz, P.: Vertical profiling of Saharan dust with Raman lidars and airborne HSRL in southern Morocco during SAMUM, Tellus B, 61, 144-164, doi:10.1111/j.1600-0889.2008.00390.x, 2009b.

Vaughan, M. A., Young, S. A., Winker, D. M., Powell, K. A., Omar, A. H., Liu, Z., Hu, Y. and Hostetler, C. A.: Fully automated analysis of space-based lidar data: An overview of the CALIPSO retrieval algorithms and data products, Proc. SPIE 5575, Laser Radar Techniques for Atmospheric Sensing, 16, doi:10.1117/12.572024, 2004.

Vaughan, M. A., Powell, K. A., Kuehn, R. E., Young, S. A., Winker, D. M., Hostetler, C. A., Hunt, W. H., Liu Z., McGill, M. J. and Getzewich, B. J.: Fully automated detection of cloud and aerosol layers in the CALIPSO lidar measurements, J. Atmos. Ocean Technol., 26, 2034-2050, doi:10.1175/2009JTECHA1228.1, 2009.

Wang, M. and Penner, J.: Aerosol indirect forcing in a global model with particle nucleation, Atmos. Chem. Phys., 9, 239-260, doi:10.5194/acp-9-239-2009, 2009.

Westervelt, D., Moore, R., Nenes, A. and Adams, P.: Effect of primary organic sea spray emissions on cloud condensation nuclei concentrations, Atmos. Chem. Phys., 12, 89-101, doi:10.5194/acp-12-89-2012, 2012.

Winker, D. M., Vaughan, M. A., Omar, A., Hu, Y., Powell, K. A., Liu, Z., Hunt, W. H. and Young, S. A.: Overview of the CALIPSO mission and CALIOP data processing algorithms, J. Atmos. Ocean. Technol., 26, 2310-2323, doi:10.1175/2009JTECHA1281.1 2009.

Young, S. A., Cutten, D. R., Lynch, M. J. and Davies, J. E.: Lidar-derived variations in the backscatter-to-extinction ratio in southern hemisphere coastal maritime aerosols, Atmos. Environ., 27, 1541-1551, doi:10.1016/0960-1686(93)90154-Q, 1993.

Young, S. A. and Vaughan, M. A.: The retrieval of profiles of particulate extinction from cloud-aerosol lidar infrared pathfinder satellite observations (CALIPSO) data: algorithm description, J. Atmos. Oceanic Technol., 26, 1105-1119, doi:10.1175/2008JTECHA1221.1, 2009.

Tables

Table 1. Seasonal means and standard deviations (in parenthesis) for 2° × 5° grid cell medians. The subscripts p, S, and C appended to τ stand for particulate, SODA, and CALIOP, respectively, where τ is the AOD.

Season	SODA $\tau_{p,S}$	CALIOP $\tau_{p,C}$	Γ_p,× 10^{-3} sr^{-1}	S_p sr
Winter	0.14 (0.04)	0.09 (0.03)	4.7 (1.2)	27 (8)
Spring	0.13 (0.03)	0.09 (0.03)	4.8 (1.2)	24 (7)
Summer	0.14 (0.04)	0.09 (0.03)	4.6 (1.2)	27 (8)
Fall	0.13 (0.03)	0.09 (0.03)	4.7 (1.1)	25 (7)

Table 2. Means and standard deviations (in parenthesis) for 2° × 5° grid cell medians for various AMSR-E wind speed regimes. The subscripts S and C appended to τ stand for SODA and CALIOP, respectively, where τ is the AOD.

Wind Regime ms^{-1}	SODA τ_S	CALIOP τ_C	Γ_p,× 10^{-3} sr^{-1}	S_p sr	Number (%)
$0 < U_{10} \leq 4$	0.12 (0.05)	0.07 (0.04)	3.6 (1.4)	32 (17)	11849 (5)
$4 < U_{10} \leq 6$	0.11 (0.04)	0.07 (0.03)	3.8 (1.1)	27 (12)	32899 (13)
$6 < U_{10} \leq 8$	0.12 (0.04)	0.08 (0.02)	4.2 (1.0)	26 (9)	60083 (23)
$8 < U_{10} \leq 10$	0.13 (0.03)	0.08 (0.02)	4.7 (1.0)	26 (7)	68899 (26)
$10 < U_{10} \leq 12$	0.15 (0.04)	0.10 (0.03)	5.1 (1.0)	26 (6)	45895 (17)
$12 < U_{10} \leq 15$	0.16 (0.04)	0.12 (0.03)	5.7 (1.2)	25 (6)	30162 (11)
$U_{10} > 15$	0.16 (0.04)	0.14 (0.04)	6.4 (1.4)	22 (7)	12953 (5)

Figures

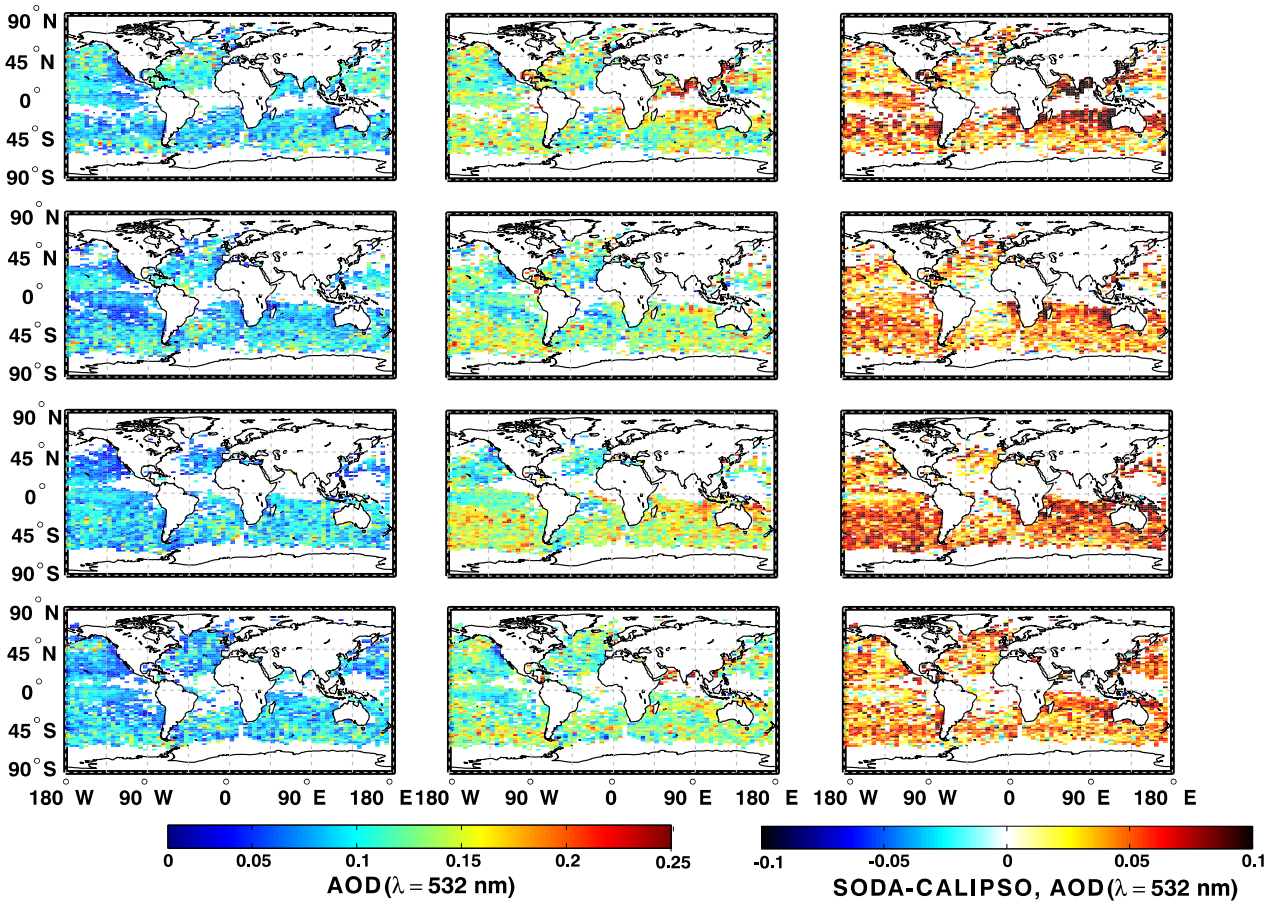

Fig. 1 - Seasonal median AOD values from CALIOP and SODA (columns 1 and 2) and the difference (SODA – CALIOP) plot (column 3) for December - February (row 1), March - May (row 2), June - August (row 3), September - November (row 4) plotted on a 2° × 5° latitude longitude grid. "No Data" is shaded white and is defined as grid cells failing quality control algorithm (see text for details).

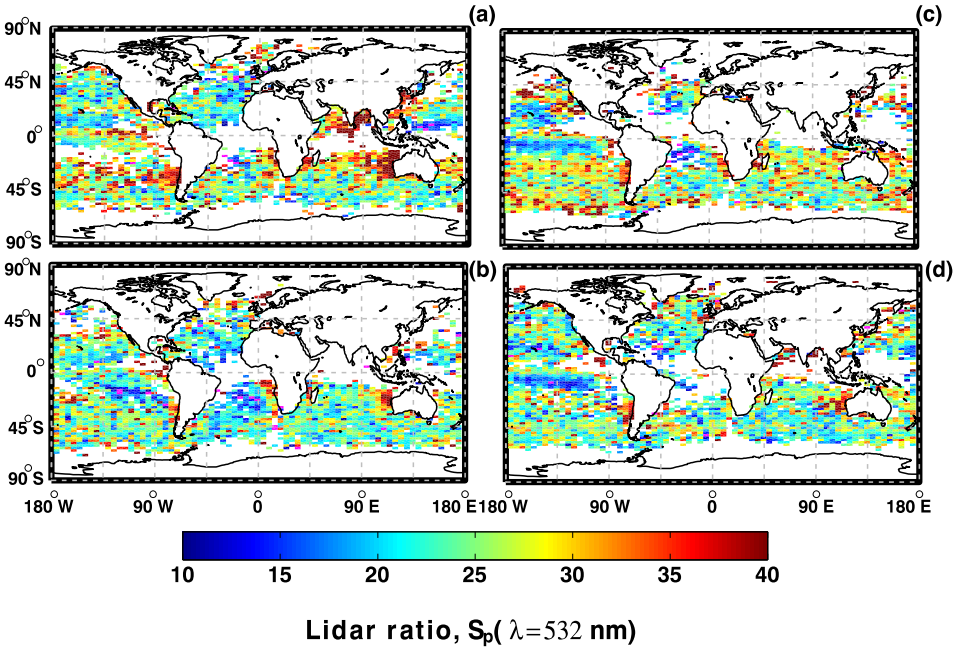

Fig. 2 - Seasonal lidar ratio for 2° × 5° latitude longitude grid cells. Seasons are arranged as (a) December - February , (b) March - May, (c) June - August, (d) September - November.

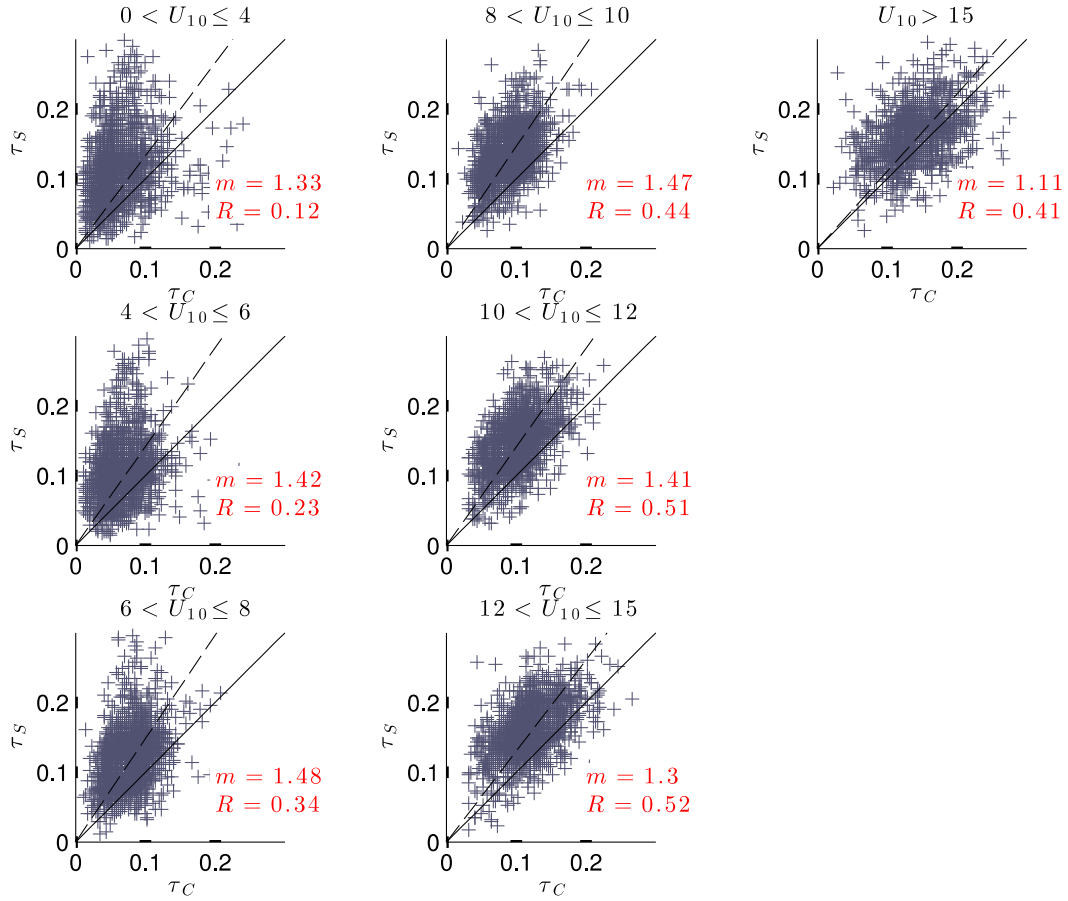

Fig. 3 - Scatter plot of SODA ($\boldsymbol{\tau_S}$) to CALIOP ($\boldsymbol{\tau_C}$) AOD for each wind speed regime. Each crosshair indicates a grid cell median. The black solid and dashed lines indicate the 1:1 and least squares estimator lines respectively. Slopes (m) and correlation coefficients (R) are also reported.

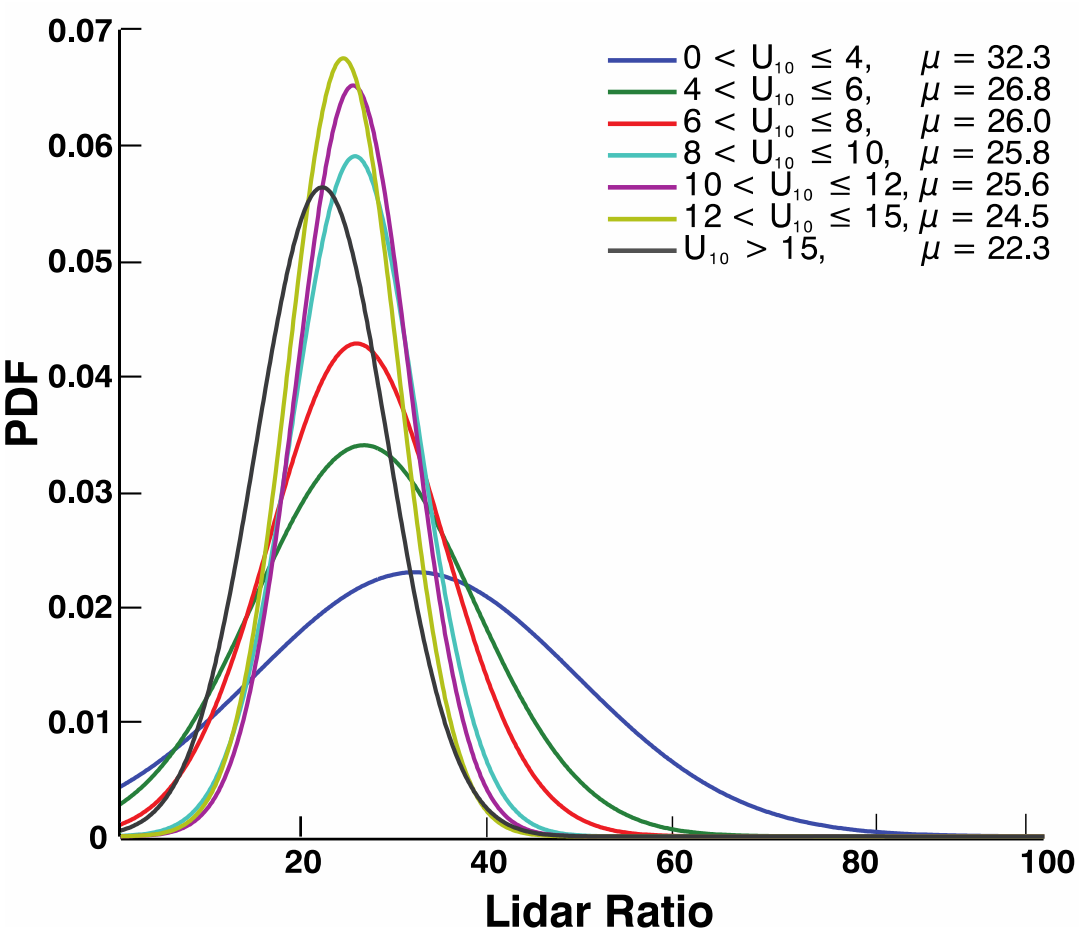

Fig. 4 - Probability density function of clean marine aerosol lidar ratio for selected AMSR-E wind speed regimes. The mean (μ) of each distribution is also reported.

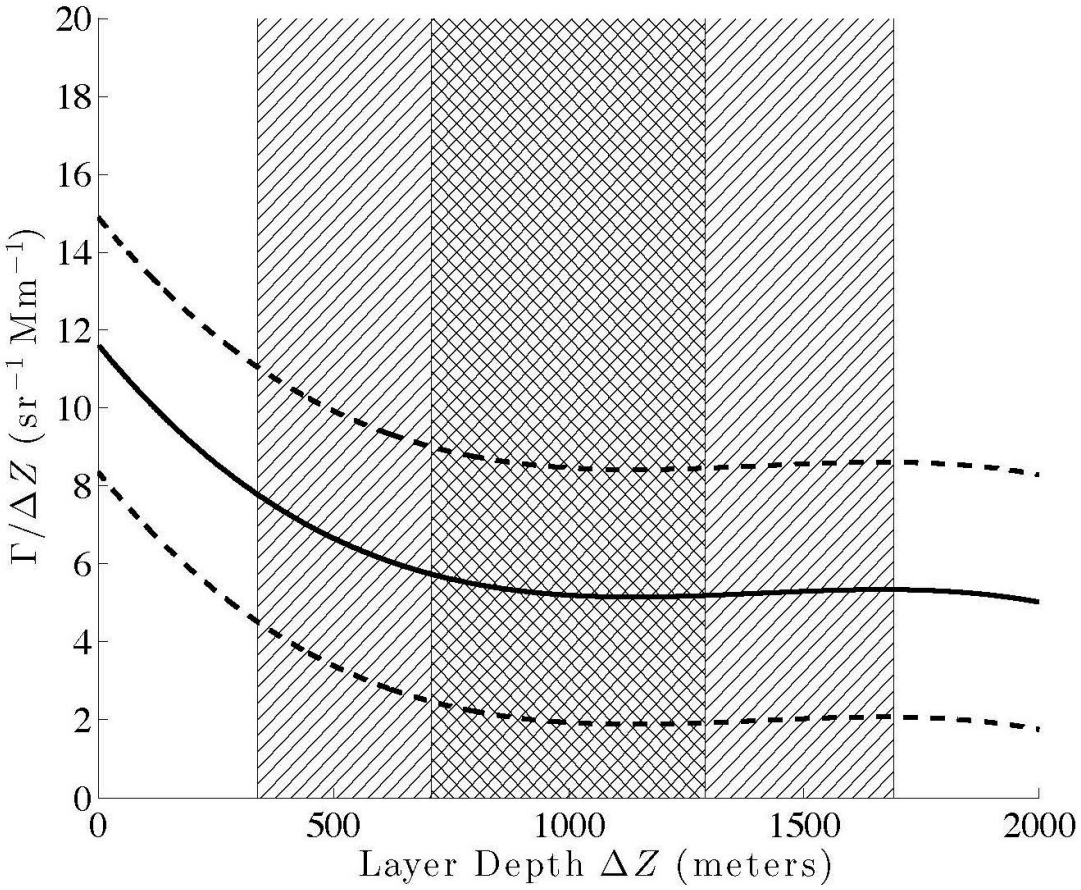

Fig. 5 - The normalised integrated attenuated backscatter as a function of the layer depth. The solid line shows the 3rd order least squares fit to the data while the dotted lines show +/- 1$\boldsymbol{\sigma}$; the hatched area shows the layer depth data frequency: cross hatch between the 25th and 75th percentiles and straight hatch between 5th and 95th percentiles.

Supplementary Information

Table S1. Common techniques for measuring the lidar ratios along with some values reported for marine aerosol at 532 nm wavelength.

Instrumentation	Operating Principle	$S_{p,532}$ (sr)
Raman Lidar[(b)]	Light is scattered at a different wavelength than the incident laser. Aerosol extinction is calculated by the Raman lidar equation. Rayleigh coefficients for molecular attenuation are calculated with measured or modeled temperature and pressure profiles. The ratio of inelastic (shifted wavelength due to aerosol scattering) backscatter to the elastic (same wavelength) backscatter determines the aerosol backscatter. The particulate lidar ratio is then the aerosol extinction-to-backscatter.	23 ± 3[(a)] 23 ± 5[(a)] 18 ± 2[(c,d)]
HSRL Lidar[(h)]	Cabannes scattering broadens the molecular scattering channel with the tails removed by a narrow bandwidth iodine filter that only passes the aerosol return. The backscattered aerosol return is then used along with Rayleigh parameters calculated by atmospheric temperature and pressure profiles to calculate aerosol extinction. The particulate lidar ratio is then the aerosol extinction-to-backscatter.	18 ± 5[(e)] $15 - 25$[(f)] $17 - 27$[(g)]
Modeled with measured size distributions[(i)]	The aerosol size distribution is measured and used with Mie theory (with an assigned or measured refractive index) to retrieve aerosol extinction and backscatter and thereby the lidar ratio. AERONET (Holben et al., 1998) uses an inversion procedure from radiance data collected by sun photometers to derive the aerosol size distribution.	28^{*}[(i)] 25.4 ± 3.5[(j)] 29^{**}[(k)]
Phase function and single scattering albedo measurements[(l)]	The lidar ratio is also written as the inverse of the single scattering albedo and phase function at 180°. Passive instruments like the POLarization and Directionality of the Earth's Reflectances (POLDER) radiometer retrieve aerosol scattering at multiple angles to determine the phase function and retrieve the lidar ratio. This can also be done with lidar and backscattering nephelometers.	25[(l)]

[(a)] Müller et al. (2007); [(b)] Ansmann and Müller (2005); [(c,d,e)] Groß et al. (2011a; 2011b; 2013); [(f,g)] Burton et al. (2012; 2013); [(h)] Hair et al. (2008); [(i)] Sayer et al. (2012); [(j)] Masonis et al. (2003); [(k)] Cattrall et al. (2005); [(l)] Bréon (2013). * signifies a suggested value, and ** signifies 550 nm.

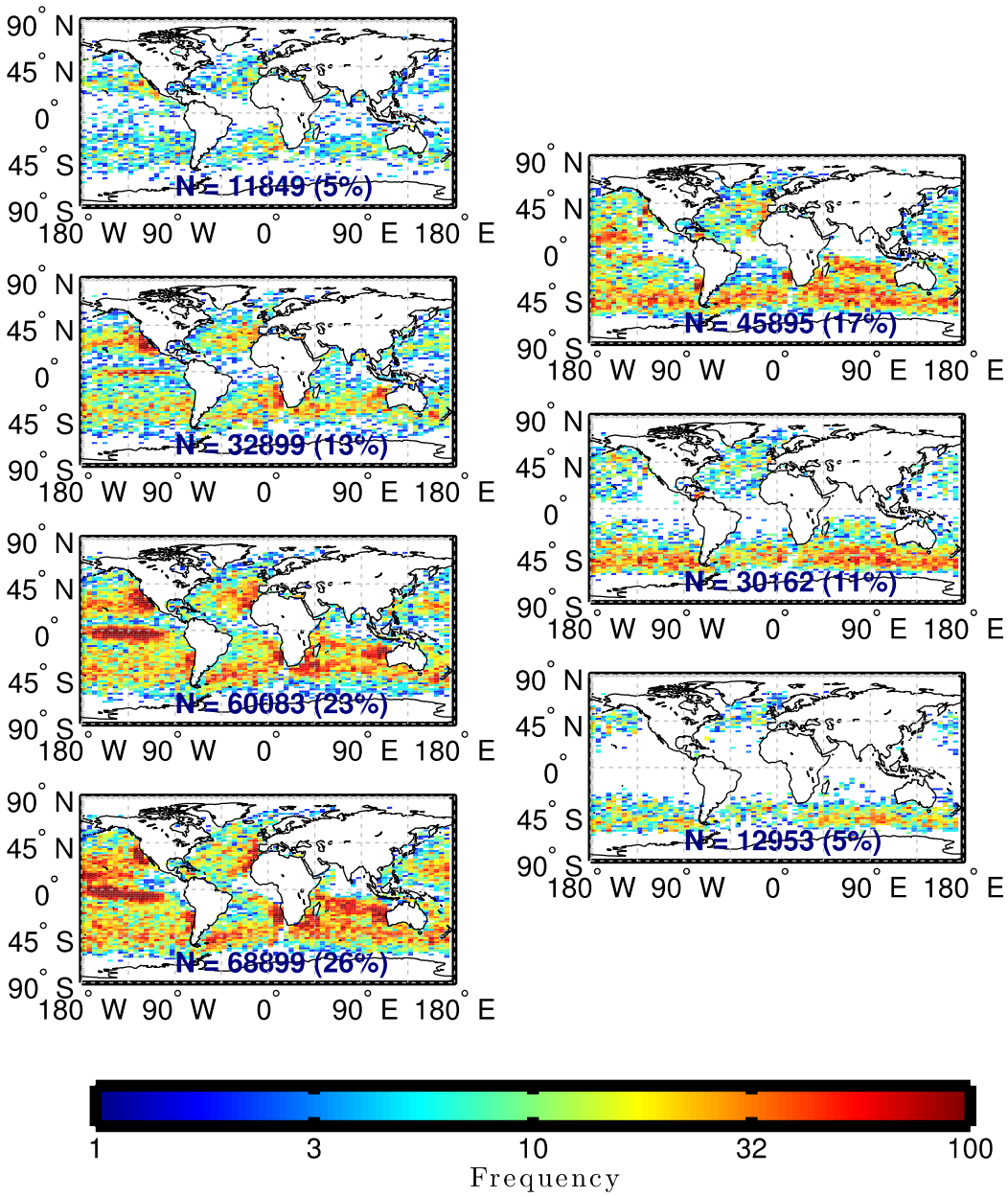

Fig S1. CALIOP retrieval counts for each 2° × 5° latitude longitude grid cell and different wind speed regimes. Total number and percent of total (in parenthesis) is also reported for each wind regime. Wind speed regimes for column 1 from top to bottom, are 0-4, 4-6, 6-8, and 8-10 m s^{-1} and column 2 from top to bottom are 10-12, 12-15, and >15 m s^{-1}.

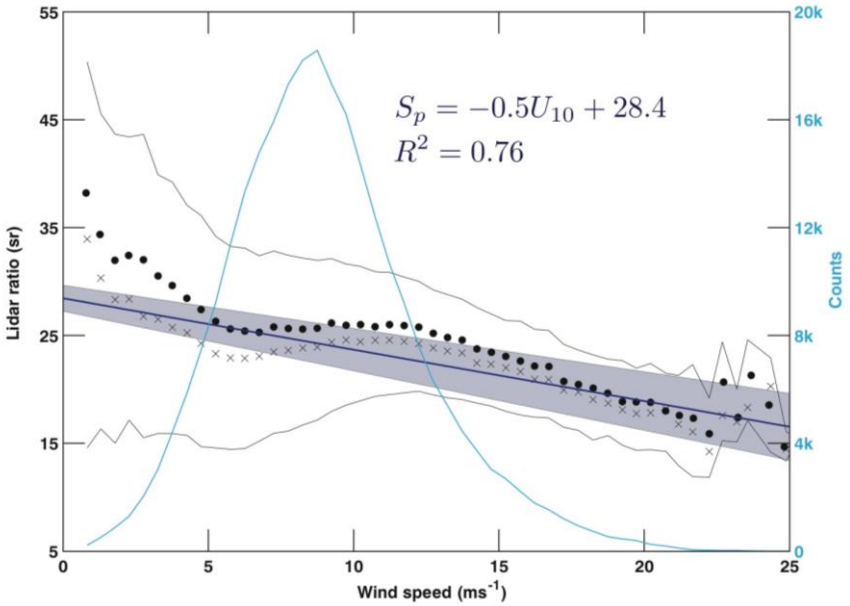

Fig S2. Median lidar ratio as a function of wind speed (dark blue line). The solid black lines correspond to the 25th (lower) and 75th (upper) percentiles for each data point. Black crosses (dots) are median (mean) lidar ratios for each wind speed bin at 0.5 ms^{-1} intervals. The light blue line corresponds to the number of retrievals shown on the y-axis to the right. The equation for the least squares linear regression is $S_p = -0.5U_{10} + 28.4$ with an $R^2 = 0.76$. The shaded region is the 95% confidence interval of the fit.